J Mater Sci: Mater Med (2010) 21:1109–1120
DOI 10.1007/s10856-009-3974-z

Mechanical properties of hydroxyapatite–zirconia compacts sintered by two different sintering methods

Declan J. Curran · Thomas J. Fleming · Mark R. Towler · Stuart Hampshire

Received: 28 September 2009 / Accepted: 9 December 2009 / Published online: 27 December 2009

Abstract Microwave sintering is traditionally employed to reduce the sintering temperature required to densify powder compacts. The effect of microwave heating on hydroxyapatite (HA)–zirconia (ZrO_2) green bodies has been investigated in order to understand how microwave energy may affect the physical and mechanical properties of the resultant densified composites. Laboratory synthesised nano-sized HA and a commercial nano-sized ZrO_2 powder have been ball milled to create mixtures containing 0–5 wt% ZrO_2 loadings. Compacts were microwave sintered at either 700, 1000 or 1200°C with a 1 h hold time. Comparative firings were also performed in a resistive element furnace using the same heating profile in order to assess the differences between conventional and microwave heating on the physical, mechanical and microstructural properties of the composites. Samples sintered at 700°C show little sign of densification with open porosities of approximately 50%. Composites conventionally sintered at 1000°C were between 65 and 75% dense, whereas the samples microwave sintered at this temperature were between 55 and 65% dense. Samples sintered at 1200°C showed the greatest degree of densification (>80%) with a corresponding reduction in open porosities. TCP generation occurred as a consequence of sintering at 1200°C, even with 0 wt% ZrO_2, and increased degradation of the HA phase to form significant amounts of TCP occurred with increasing additions of ZrO_2, along with increasing open porosity. Nanosized ZrO_2 prevents the densification of the HA matrix by effectively pinning grain boundaries and this effect is more pronounced in the MS materials. Similar strengths are achieved between the microwave and conventionally sintered samples. Greater amount of open porosity and pore interconnectivity are seen in the MS samples, which are considered to be useful for biomedical applications as they can promote osteo-integration.

D. J. Curran · T. J. Fleming · M. R. Towler · S. Hampshire
Materials and Surface Science Institute, University of Limerick, National Technological Park, Limerick, Ireland

M. R. Towler (✉)
The Inamori School of Engineering, Alfred University, Saxon Drive, Alfred, NY 14802, USA
e-mail: Towler@Alfred.edu

1 Introduction

Due to its resemblance to the mineral component of bone and teeth and its bio-compatibility [1, 2], hydroxyapatite (denoted hereafter as HA) [$Ca_{10}(PO_4)_6(OH)_2$)] is used in an increasing number of medical applications. HA has been shown to be both bio-compatible [3] and osteo-conductive [4–6], allowing it to promote the growth of new bone in-vivo without eliciting an immune response. The low mechanical strength and the inherent brittleness of HA have excluded its employment as a load bearing implant and have restricted its use to that of a bioactive layer on metallic/plastic porous implant materials to promote bone growth, and also non-load bearing applications such as ossicles in the middle ear [7, 8].

Sintering HA at high temperatures can result in the formation of calcium phosphate based decomposition products such as tetracalcium phosphate [TTCP] {$Ca_4(PO_4)_2O$} which can further degrade to tri-calcium phosphate [TCP] {$Ca_3(PO_4)_2$} [9] and calcium oxide [CaO]. These secondary phases have, in certain instances, been reported to adversely affect biological response [10, 11].

Zirconia (ZrO_2) based ceramics have been gaining much attention in recent years [12, 13] because of their relatively high fracture toughness compared with other ceramics.

ZrO_2 is a relatively bio-inert material and as such, ZrO_2 and ZrO_2 toughened ceramics have been used as components in femoral head replacement prostheses [14, 15] and as dental restorative materials due to suitable aesthetics and wear resistance [16]. Several ceramic materials benefit from the addition of ZrO_2 inclusions to improve their hardness/toughness and wear characteristics, including alumina (ZrO_2 toughened alumina, ZTA) and mullite (ZrO_2 toughened mullite, ZTM) [16, 17]. Initial work by Towler et al. [18] has shown that the mechanical properties of HA can also be improved using ZrO_2 inclusions.

High sintering temperatures (>1500°C) are required in order to fully densify ZrO_2. Producing dense HA–ZrO_2 composite bodies can be problematic as these high temperatures and can lead to dehydroxylation and subsequent decomposition of HA to calcium phosphate forms which are either brittle or more resorbable in-vivo [1, 19, 20]. In this work, HA/ZrO_2 composites have been fabricated from nano-sized powders in order to reduce the sintering activation energies necessary to cause densification. In addition, a microwave sintering regime has been employed as microwaves can be used to densify ceramics to near 100% theoretical density (TD) using lower sintering temperatures and shorter soaking times than with conventional sintering [21–24]. Microwave energy has also been shown to produce ceramics with altered phase assemblages and microstructures [25, 26]. It is possible that microwave sintering may provide a method to produce a composite which is more favourable to osteo-integration [27, 28] due to an increased level of open porosity [27] and increased interconnected porosity [6, 29, 30].

2 Materials and methods

Pure HA powder was produced at a synthesis temperature of 25°C based on a simple precipitation method [31]. 78.72 g (0.3335 mol) of calcium nitrate hydrated ($Ca(NO_3)_2{\cdot}4H_2O$) in 600 ml of water was made basic by the addition of 10 ml of ammonium hydroxide (NH_4OH). 26.41 g (0.2000 mol) of di-ammonium hydrogen orthophosphate ($(NH_4)_2HPO_4$) was made basic in 1066 ml of water by the addition of 25 ml of NH_4OH. The $Ca(NO_3)_2{\cdot}4H_2O$ and $(NH_4)_2HPO_4$ solutions were brought to the desired synthesis temperature and stirred vigorously before synthesis to ensure the reagents were completely dissolved. To determine this, visual inspections of the solution were conducted for un-dissolved reagent particulates. Under continued vigorous stirring, the $(NH_4)_2HPO_4$ solution was added drop-wise from a glass funnel into the $Ca(NO_3)_2{\cdot}4H_2O$ solution over a 60 min interval. Throughout the synthesis the pH was kept above 10.0 by the addition of NH_4OH at constant intervals to avoid shock to the system. Once the drop-wise addition was completed, the solution was kept at the synthesis temperature of 25°C for 1 h under vigorous stirring conditions, effectively allowing an ageing time of 1 h [31]. The sample was then left to stand for 24 h at room temperature. The supernatant was removed and replaced with fresh distilled water, re-stirred for 1 h and left to stand again for 24 h. This procedure was undertaken three times to remove any unwanted residue from the precipitate. The supernatant was removed a final time and replaced with distilled water and spun for 15 min. The suspension was then filtered under vacuum, using a Buchner filter and distilled water until the ammonia was removed. The filter cake was then removed from the filter and placed into a beaker and dried in a fan assisted oven at 85°C for 20 h.

2.1 Particle size analysis

A laser diffraction technique (Malvern Mastersizer 2000, Malvern Instruments Ltd., Malvern, UK) was employed in order to measure the particle size distribution of the HA. Approximately 25 ml of a suspension of HA powder was added drop-wise to the sample tank, which was filled with distilled water, resulting in a measured obscuration of approximately 9%. The solution was subject to ultrasonic and mechanical agitation for the duration of the measurement cycle in order to eliminate any soft agglomerates and to ensure even dispersion throughout the sample tank. Ten individual measurements were made for each sample. The particle size distribution (median particle size, d_{50}, along with the diameter of the particles at 10% (d_{10}), and 90% (d_{90}) of the cumulative frequency curve) was recorded.

The surface area of the HA powder was evaluated using the BET method (Micrometrics ASAP 2010, USA) utilising nitrogen as the adsorbate. The samples were de-gassed overnight at 120°C under vacuum. Assuming that the particles have a spherical shape with a smooth surface and a similar size, the surface area can be related to the average particle size using the following geometrically derived equation:

$$D_{BET} = 6000/(\rho \cdot S_{BET}) \quad (1)$$

where D_{BET} is the average particle size (nm), P the density (g/cm^3) and S_{BET} the specific surface area (m^2/g).

2.2 Crystallite size and morphology

TEM (JEM-2011, Jeol, Japan) of the HA suspension was undertaken in order to investigate the crystallite morphology and to verify the particle size information from the laser diffraction technique. A drop of the HA suspension prior to drying was placed on a copper grid before imaging with a 200 kV electron beam.

2.3 Calcium phosphate ratio

The calcium to phosphorus ratio and the trace element impurity content of the prepared HA were determined by X-ray fluorescence (XRF) (Ceram Research Ltd., Stoke on Trent, UK).

2.4 Phase purity

X-ray diffraction (XRD) was performed using a Philips X'Pert PRO MPD diffractometer (Panalytical, Royal Philips Electronics, The Netherlands) over a range of $5° < 2\theta < 80°$ with a step size of 0.017° and a time per step of 20.029 s.

2.5 HA–ZrO_2 composite sample preparation

Pure ZrO_2 powder (99.9+% purity ZrO_2) was sourced from Tosoh Corporation (Nanyo Manufacturing Complex, Yamaguchi, Japan) and mixed with the HA by using a dry ball-milling technique with alumina media for 6 h to create batches of composite powders with 1, 2, 3, 4 and 5 wt% ZrO_2 addition. BET (Micromeritics ASAP 2010, USA) was performed in order to determine the surface area of the resultant powder. To create test bodies, 1.5 g of the composite powders were uniaxially pressed into 20 mm ø discs in a stainless steel die.

Back scattered SEM and EDX (Joel JSM-840-SEM, Joel, Japan) utilising a 20 keV beam was performed on the green bodies in order to examine the dispersion of ZrO_2 particles in the HA. The green bodies were then densified using a conventional resistive element furnace and a microwave sintering furnace.

2.6 Sintering

Microwave sintering was performed in a hybrid microwave sintering furnace developed at the University of Limerick (Limerick, Ireland). The device has a peak microwave power output of 1.125 kW and utilises silicon carbide (SiC) as a susceptor medium to facilitate hybrid heating. This method minimises thermal gradients within the sample, whilst providing the ability to heat the samples to a critical temperature beyond which they heat solely due to microwave radiation absorption. Firings were performed at 700, 1000 and 1200°C (±20°C, 1 h hold) and subsequently left to furnace cool. Comparative firings with the same heating profile as in the microwave sintering furnace were performed in a conventional resistive element furnace.

2.7 Density and porosity

The densities and open porosities of the sintered bodies were measured using an immersion method. Samples were weighed in air and then placed under high vacuum for 1 h. Water was introduced into the vacuum system without breaking the vacuum. The samples were left for 2 h under vacuum to allow the water to penetrate the pores. The samples were then removed from the vacuum and excess water was absorbed from the surface using absorbent paper. The samples were then weighed in air and subsequently in water.

Sample specific gravity (density) was calculated by the formula:

$$\rho\left(\mathrm{g/cm^3}\right) = \frac{W_a \cdot [\rho_{fl} - 0.0012]}{0.99983 \cdot G} + 0.0012 \quad (2)$$

where W_a is the weight of sample in air (g), G is $W_a - W_{fl}$, W_{fl} the weight of sample immersed in water, ρ_{fl} the density of water at specific temperature.

The percentage relative density (% RD) was then calculated using:

$$\text{Composite RD}(\%) = \frac{\rho}{(\text{TD HA} \times \text{wt\% HA}) + (\text{TD } ZrO_2 \times \text{wt\% } ZrO_2)} \times 100 \quad (3)$$

where density of water = 0.99823 g/cm^3 (at 20°C), theoretical density (TD) HA = 3.156 g/cm^3 and theoretical density (TD) ZrO_2 [32] = 6.156 g/cm^3.

2.8 Vickers microhardness

Vickers Hardness measurements were performed using a diamond indentation technique (Leco M-400-G1 Hardness Tester, Michigan, USA). The samples sintered at 1200 and 1000°C were indented with a 100 g load for 15 s, and the samples sintered at 700°C were indented with a 50 g load for 15 s. The resultant indents (n = 15 per composition, across six different samples) were measured and used to calculate hardness using the following formula:

$$H_v = \frac{2P\ \mathrm{Sin}\theta/2}{d^2} \quad (4)$$

where H_v is the Vickers hardness, P the applied load, θ the apex angle of the indenter and d the mean of the measured indenter diagonals.

2.9 Bi-axial flexural strength

Bi-axial flexural strength measurements were performed using a modification of ISO 6872 [33]. A load frame (Lloyd LR50K, Lloyd Instruments, UK) with a crosshead speed of 0.1 mm/min was utilised along with a suitable bi-axial flexural strength test jig with support radius of 8 mm (Fig. 1).

Fig. 1 Bi-axial flexural strength test jig

2.10 Fracture surface SEM

SEM and energy dispersive X-ray analysis (EDX) (SU70 FE-SEM, Hitachi High-Technologies Europe GmbH, Krefeld, Germany) were performed on the fracture surfaces generated as a result of bi-axial flexural strength testing.

3 Results

3.1 Particle size analysis

The particle size distribution, as measured using a laser diffraction technique, is presented in Fig. 2, it indicates that the synthesised HA has a narrow particle size distribution centred at $d_{50} = 0.192$ µm.

BET measurements (S_{BET}) indicate that the HA powders have specific surface areas of ~ 151 m^2/g.

Solving for S_{BET} in Eq. 1 results in a value of ~ 0.013 µm, which is 10% of the measured d_{50} value. This indicates that sonication is insufficient to disrupt all agglomerates.

3.2 Crystallite size and morphology

Figure 3 is a typical TEM image of the HA. Individual crystals are of the order of 10 nm in size.

Comparing the TEM and PSA results it is apparent that the nanosized crystallites are agglomerated into micron sized clumps.

3.3 Calcium phosphate ratio

Results of XRF analysis performed on the precipitated HA are presented in Table 1. The Ca/P ratio was 1.66, indicative of stoichiometric HA. XRF also indicates that there are minimal amounts of contaminants present.

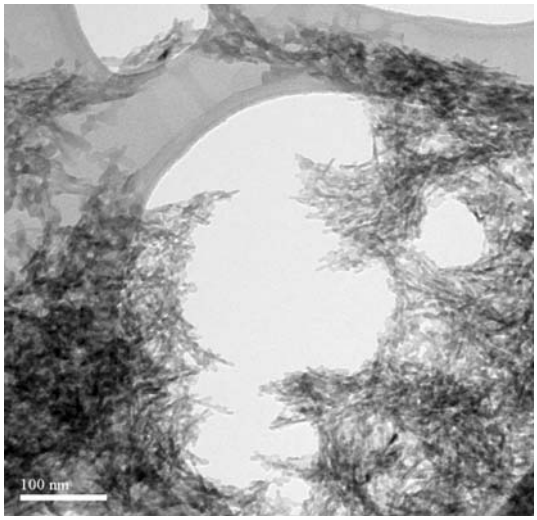

Fig. 3 TEM image of HA crystallites synthesised at 25°C deposited on a copper substrate

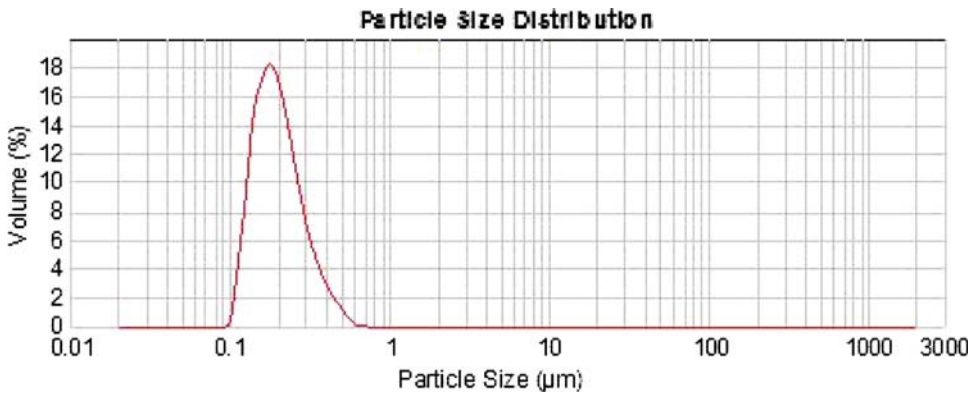

Fig. 2 Particle size distribution of HA synthesised at 25°C

Table 1 XRF elemental analysis (only main components are shown)

Results	Element	Amount (%)
Calcium oxide	CaO	52.51
Phosphorus pentoxide	P_2O_6	40.52
Magnesium oxide	MgO	0.12
Sodium oxide	Na_2O	<0.03
Zirconium oxide	ZrO_2	<0.02
Lead oxide	PbO	<0.02
Ca/P ratio		1.66

3.4 Phase purity

Figure 4 shows the XRD pattern for the HA synthesised at 25°C and that for JCPDS card number 9-0432, denoted HA with the formula $Ca_5(PO_4)_3(OH)$, which was the best matching pattern found in the index. This is an indexed quality card and is a standard for the determination of HA [34–36].

The major identification peaks of HA and the equivalent values of 2θ are for the 002 (26°), 102 (28°), 200 (29°), 141 (31.5°), 122 (32°), 300 (33°), 202 (34°) and the 160 (39.5°) planes [37] each of which are present in the above scan. Rietfield analysis was performed on the obtained diffraction pattern and the unit cell parameters were found to be a = 9.429 ± 0.004 Å and c = 6.884 ± 0.003 Å.

3.5 Powder homogeneity

Back scattered SEM images of the green HA/ZrO_2 composite powders pre- and post-ball milling are shown in Fig. 5.

Prior to milling, ZrO_2 agglomerates are clearly visible as bright areas with sizes up to 100 μm. After milling, the nanosized ZrO_2 crystallites are clearly evenly dispersed throughout the HA powder.

EDX was used to verify the presence of ZrO_2 in the milled powders and the results are shown in Fig. 6. Measurements were taken of the dark HA matrix (a) and the bright ZrO_2 inclusions (b).

The presence of ZrO_2 is clearly indicated in the elemental analysis.

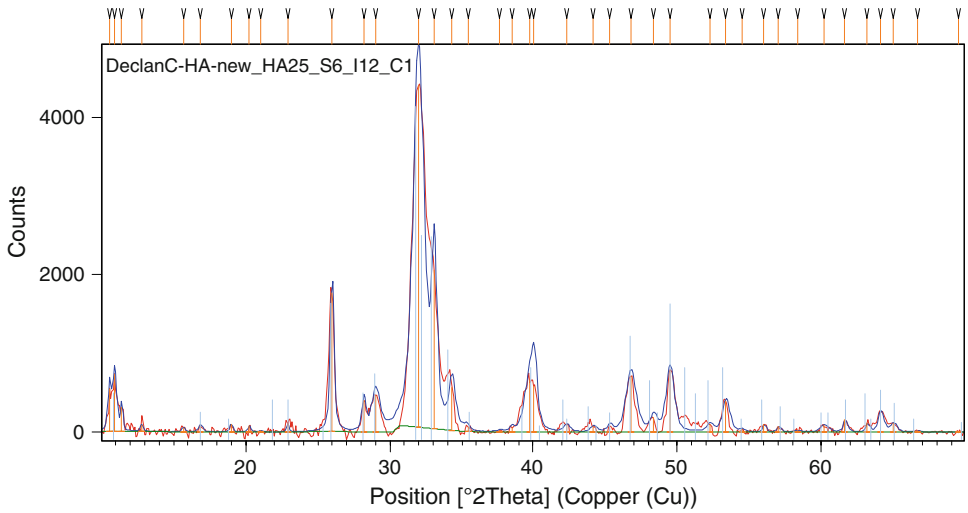

Fig. 4 X-ray diffraction peaks of HA synthesised at 25°C with overlaid JCPDS matched peaks

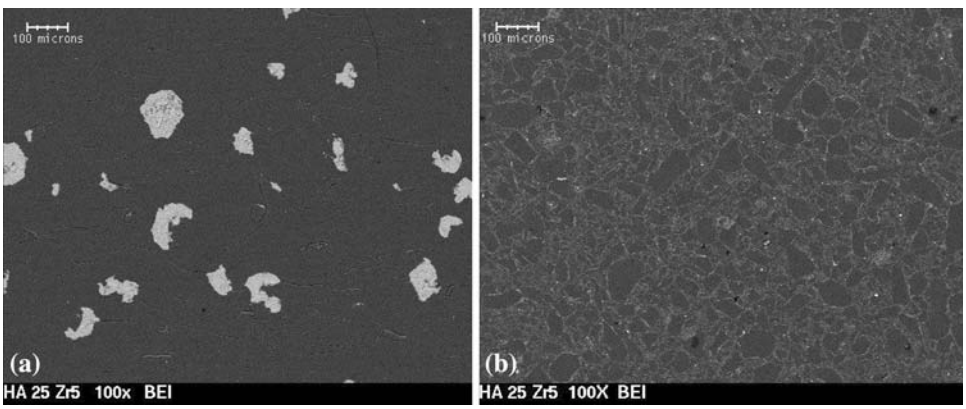

Fig. 5 Back scattered SEM image of HA/ZrO_2 powder compacts **a** pre- and **b** post-ball milling

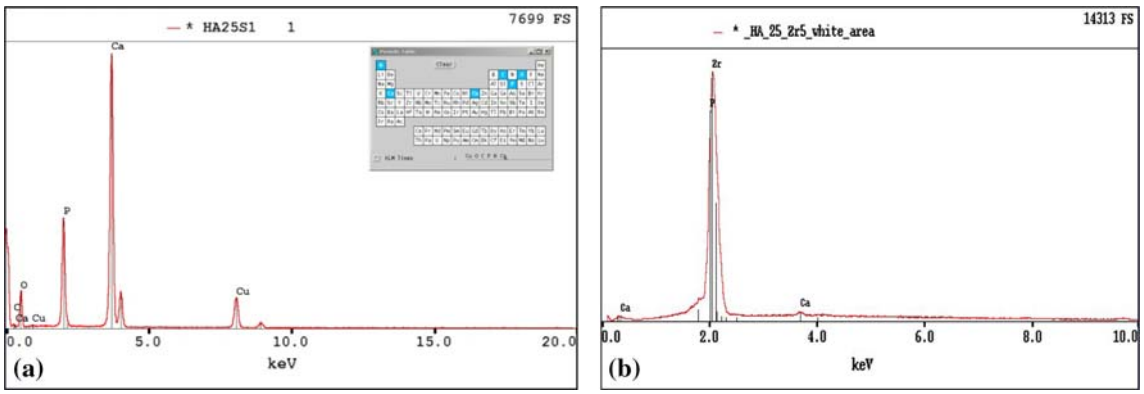

Fig. 6 EDX spectrum of ball milled HA/ZrO_2 powder, matrix (**a**) and ZrO_2 (**b**)

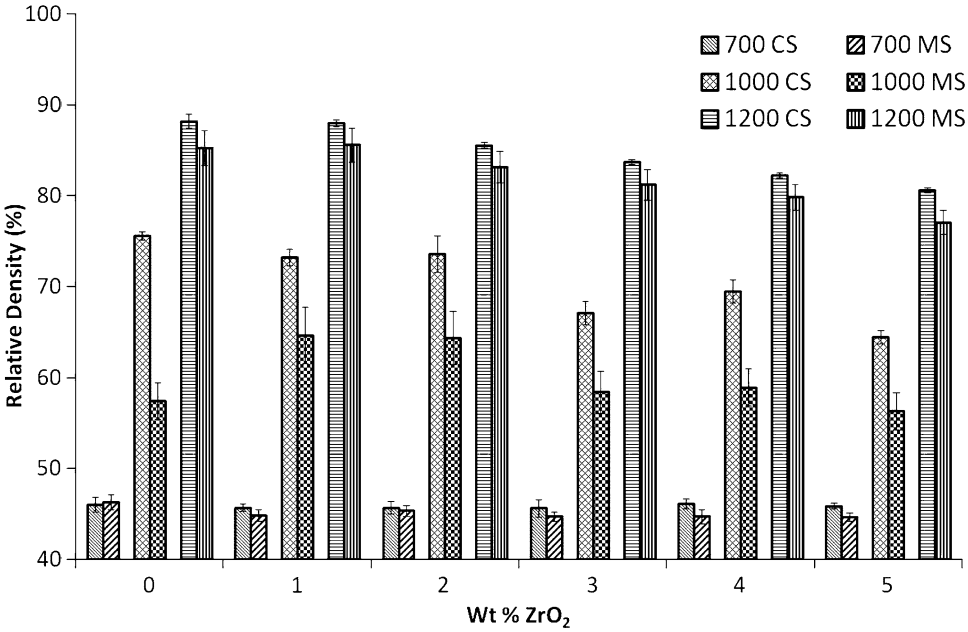

Fig. 7 % relative density of HA/ZrO_2 composites sintered at 700, 1000 and 1200°C

3.6 Density and porosity

Given the geometry and mass of the green bodies, the bulk density of the unsintered samples are of the order of 45% of the theoretical density. As a consequence of this, the green bodies possess ~55% porosity, both open and closed.

Figure 7 shows the combined plot of the % relative densities of the conventional and microwave sintered (denoted CS and MS, respectively) composite bodies sintered at 700, 1000 and 1200°C.

The relative densities of the materials sintered at 700°C are approximately 45%, similar to that of the green bodies. On increasing the sintering temperature from 700 to 1000°C there is an increase in density for each composition studied. The relative densities of CS samples decrease linearly with ZrO_2 content, from 75% at 0 wt% ZrO_2 to 65% with the addition of 5 wt% ZrO_2. The densities of the MS samples are less than their CS counterparts. The densities of the MS materials increase from 57% with 0 wt% ZrO_2 to 65% with 2 wt% ZrO_2. Additional ZrO_2 reduces the density in an almost linear fashion returning to 57% at 5 wt% ZrO_2. An increase in sintering temperature, to 1200°C, serves to increase the density of the composites further. There is a linear reduction in density with increasing ZrO_2 content regardless of heating method at this sintering temperature. There is also little statistical difference in relative densities of the CS and MS samples, which range from 86% at 0 wt% ZrO_2 to 80% at 5 wt% ZrO_2 content (Fig. 8).

The open porosities of all compositions sintered at 700°C are approximately 50%, regardless of heating method. Coupled with the density data, this indicates that

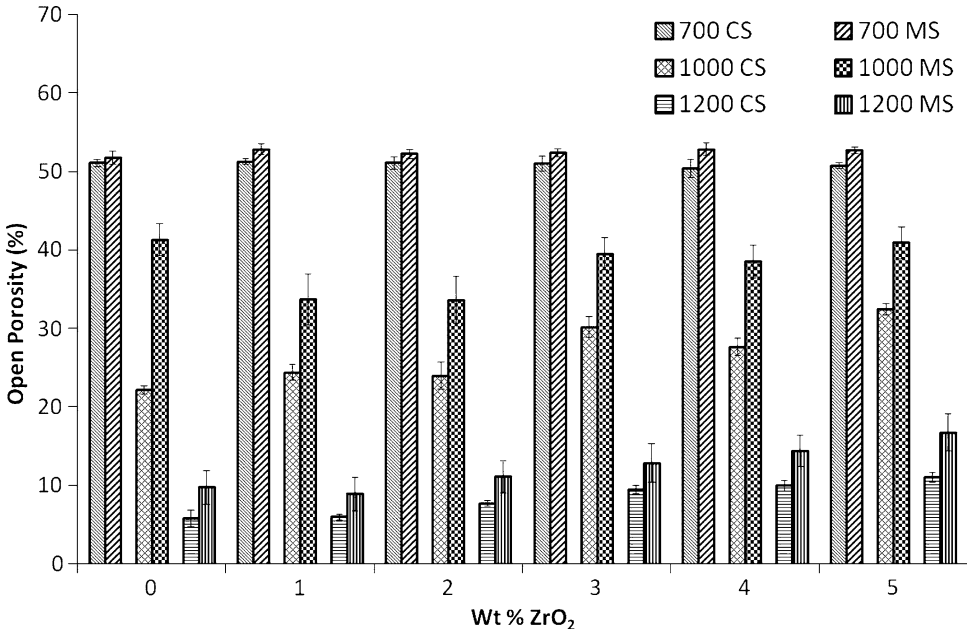

Fig. 8 % open porosities of HA/ZrO_2 composites sintered at 700, 1000 and 1200°C

this sintering temperature is insufficient to cause densification, as this degree of porosity is similar to that of a pressed green body. The open porosities of the CS composites sintered at 1000°C increases in a linear fashion from 22% at 0 wt% ZrO_2 to 32% at 5 wt% ZrO_2. The open porosities of the MS composites sintered at 1000°C do not exhibit a simple linear progression with ZrO_2 content. The bodies with 0 wt% ZrO_2 possess 41% open porosity. Subsequently the porosities increase in a linear fashion from 33% at 1 wt% ZrO_2 to 40% at 5 wt% ZrO_2. The CS samples sintered at 1200°C exhibit a slight linear increase in open porosity with increasing ZrO_2 content, ranging from 5% at 0 wt% ZrO_2 to 11% at 5 wt% ZrO_2. The MS materials sintered at this temperature follow a similar trend but contain 4% more porosity than their CS counterparts, ranging from 9% at 0 wt% ZrO_2 to 16% at 5 wt% ZrO_2.

3.7 X-ray diffraction

Quantitative X-ray analysis was performed using the X'pert Highscore software suite (Panalytical, Netherlands) in order to assess the amount of HA, ZrO_2 and possible intermediates and degradation products in the sintered bodies. This analysis was also employed to assess if the different heating methods resulted in different phase assemblages. The results of the analysis are presented in Table 2.

Without ZrO_2, small amounts (~5%) of TCP form which is consistent with previous reports [38]. Table 2 indicates that the introduction of ZrO_2 leads to significant increases in the formation of TCP compared to the 0 wt% ZrO_2 and consequent reductions in HA to levels of 75–79% for MS and 71–81% for CS samples. The 3 wt% ZrO_2 CS sample shows formation of ~5% TTCP with a reduction in HA phase compared to the MS sample. The CS samples, with 2 and 5 wt% ZrO_2 additions, show greater retention of the HA phase post sintering with levels of HA exceeding 80%. The amount of cubic ZrO_2 increases with increasing amounts of wt% ZrO_2 added.

Table 2 Quantitative X-ray analysis of MS and CS HA/ZrO_2 composites sintered at 1200°C

	wt% ZrO_2				
	0	2	3	4	5
MS					
Tetragonal ZrO_2	0.1	0.2	0	0.1	0.1
Tri calcium phosphate	5.6	20.7	20.2	22.7	19.6
Calcium zirconate	0	0.1	0	0	0
Cubic ZrO_2	0.2	0.8	0	2.4	3
Hydroxyapatite	94.1	76.1	78.8	74.7	77.1
Monoclinic ZrO_2	0	0.6	0.9	0	0
Tetra calcium phosphate	0	2	0	0	0.2
CS					
Tetragonal ZrO_2	0.4	0	0	0.1	0.1
Tri calcium phosphate	5.6	17.9	22	20.3	17
Calcium zirconate	0	0	0	0.3	0
Cubic ZrO_2	0	1.1	1.6	2.6	2.3
Hydroxyapatite	93.1	81	71.3	74.6	80.5
Monoclinic ZrO_2	0	0	0.1	0.6	0.1
Tetra calcium phosphate	0	0	5	1.6	0

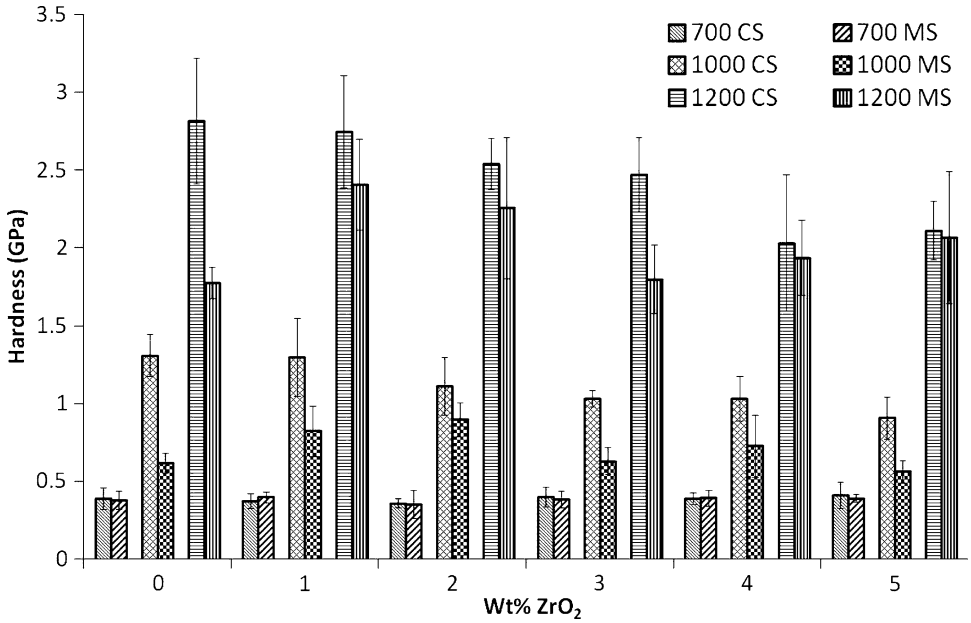

Fig. 9 Microhardness values of HA/ZrO_2 composites sintered at 1200°C

3.8 Vickers microhardness

Figure 9 shows the Vickers microhardness values for the HA/ZrO_2 composites sintered using the two different methods. It can be seen that hardness of all the compositions sintered at 700°C are ~0.40 GPa with no variation with heating method or ZrO_2 content. The hardness of the CS samples sintered at 1000°C decrease linearly with ZrO_2 content. The pure HA possesses a hardness value of 1.31 GPa which decreases to 0.91 GPa with the addition of 5 wt% ZrO_2. The hardness of the MS samples sintered at 1000°C increases from 0.62 GPa at 0 wt% ZrO_2 content to 0.89 GPa at 2 wt% ZrO_2. There is a subsequent reduction in hardness with ZrO_2 loading, decreasing to 0.56 GPa with the addition of 5 wt% ZrO_2. The hardness of the CS materials sintered at 1200°C decreases linearly with ZrO_2 content, from 2.82 GPa at 0 wt% ZrO_2, the hardest of any of the materials tested in this study, down to 2.11 GPa at 5 wt% ZrO_2 content. There is no statistical difference in the hardness of the MS samples sintered at 1200°C with mean values ranging from 1.77 to 2.4 GPa. The decreased hardness of the MS materials with respect to their CS counterparts is a reflection of the increased open porosity as exhibited by the MS samples in Fig. 8.

3.9 Biaxial flexural strength

The biaxial flexural strengths of the composites increase with increasing sintering temperature. There is little statistical difference in strengths related to the use of microwave or conventional heating methods. Also there is no statistical difference in strengths associated with ZrO_2 loading at any of the sintering temperatures studied. Composites sintered at 700, 1000 and 1200°C possess strengths of ~18, 40 and 80 MPa, respectively (Fig. 10).

3.10 Fracture surface SEM and EDX

In order to examine the microstructure of the sintered bodies, SEM images were taken of the fracture surfaces of the 0 and 5% compositions sintered at 1200°C.

For the HA (0 wt% ZrO_2) samples conventionally sintered at 1200°C, taking into account the relative density of 86% (Fig. 7) and open porosity of 5% (Fig. 8) along with the fracture surface images (Fig. 11a, b); it is apparent that these materials contain a significant amount of porosity in the form of isolated closed pores (~9%), with average isolated pore sizes in the range of 0.5–2 μm.

The microstructure of the fracture surfaces of the equivalent MS samples (Fig. 11c, d) are notably different. The open porosity has increased to ~9% with a lack of isolated pores. The bulk appears to consist of a series of "fused" grains with increased interconnected porosity and average pore sizes of less than 1 μm.

In comparison to the CS material containing 0 wt% ZrO_2 the CS composite containing 5 wt% ZrO_2 is less dense and possesses a greater degree of open porosity (~11%) (Fig. 12a, b). The CS samples do contain isolated pores with an average pore size of <1–3 μm (a). As with the materials containing 0 wt% ZrO_2, the fracture surface of the MS composite containing 5 wt% ZrO_2 consists of a series of "fused" grains with a higher degree of interconnected open porosity (~16%) (Fig. 12c, d). Smaller grains which cling to the surface of the larger features are also

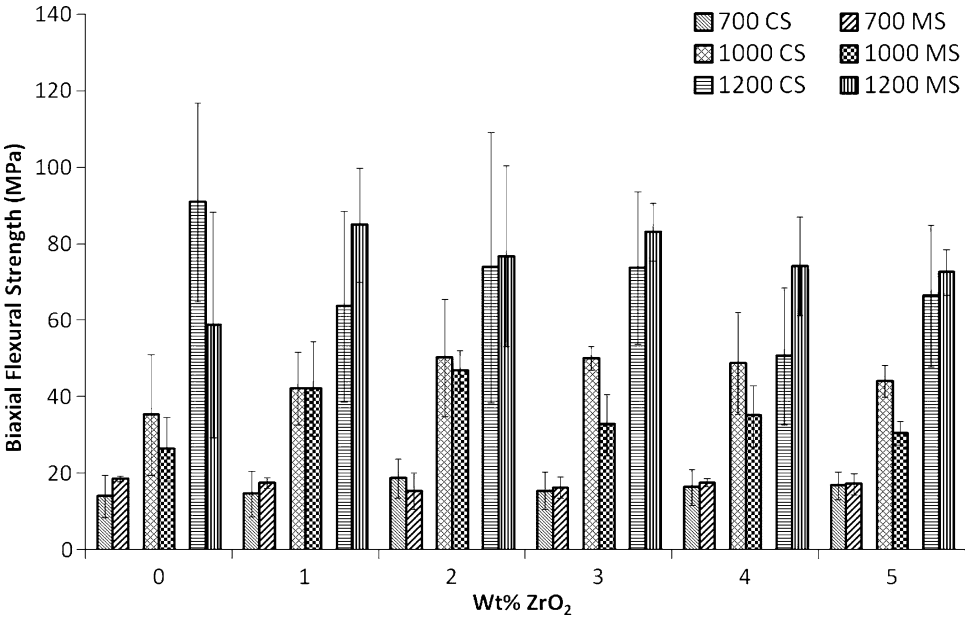

Fig. 10 Biaxial flexural strength versus wt% ZrO_2 loadings

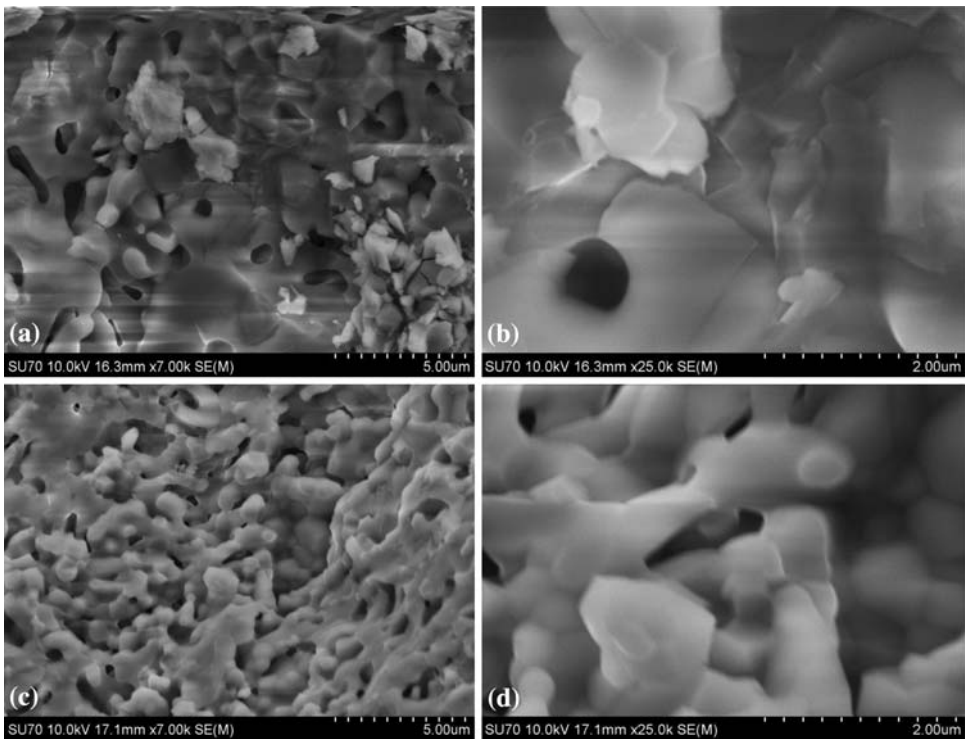

Fig. 11 SEM images of fracture surfaces of HA containing 0 wt% ZrO_2. Conventionally sintered at 1200°C, **a** ×7000, **b** ×25000. Microwave sintered at 1200°C, **c** ×7000, **d** ×25000

apparent (d) and appear as rougher regions under low magnification.

In order to investigate the relationship between the features composing the smoother and rougher areas a higher magnification image was taken.

From Fig. 13 it can be seen that the smaller grains cling to the interior surface of the pores in the underlying matrix. The increased density, lower porosity and the lack of these undensified, rougher, areas in the samples containing 0 wt% ZrO_2 suggests that the nano-sized ZrO_2 grains effectively pin the grain boundaries of the HA matrix and prevent complete densification. In order to verify this hypothesis, EDX was performed on the rough and smooth areas.

From Figs. 14 and 15, it is apparent that the dense regions contain little ZrO_2 whereas the rough porous areas containing the smaller grains contain a large proportion of ZrO_2.

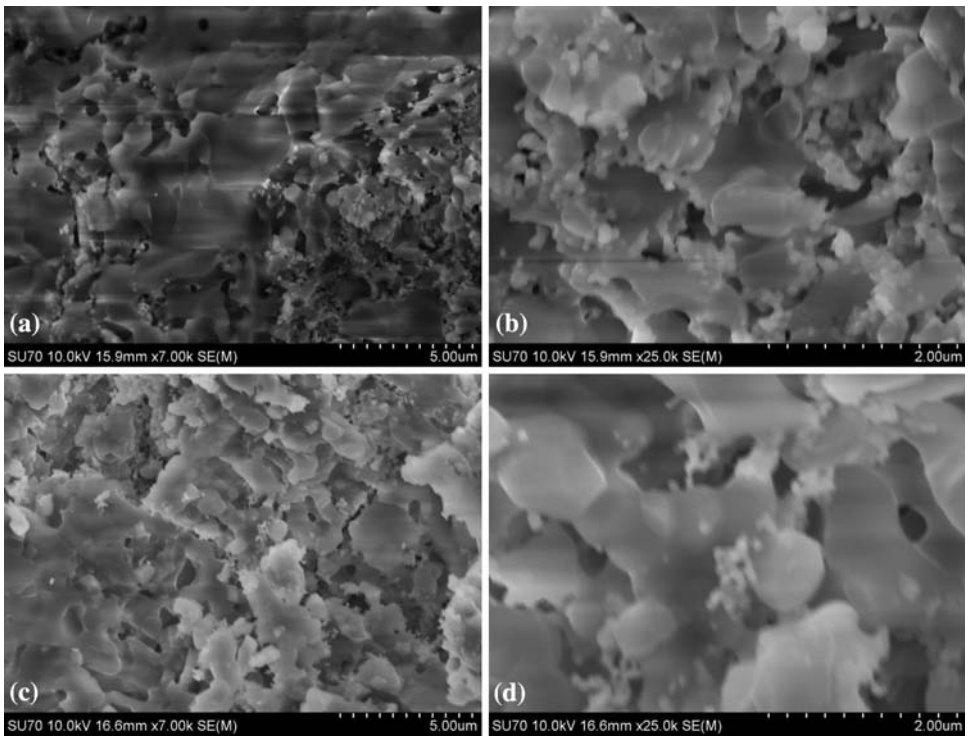

Fig. 12 Fracture surface SEM images of HA containing 5 wt% ZrO_2. Conventionally sintered at 1200°C, **a** ×7000, **b** ×25000. Microwave sintered at 1200°C, **c** ×7000, **d** ×25000

4 Discussion

From the XRF and XRD analyses, the precipitation method utilised in this study creates stoichiometric HA which is free of impurities. Particle size analysis, BET and TEM indicate that the precipitated HA powder is composed of nanosized crystallites which are clumped into sub-micron sized agglomerates. SEM and EDX analysis of the mixed powders indicates that ball milling is a suitable technique for breaking up agglomerates in the ZrO_2 powder and producing homogeneously dispersed HA–ZrO_2 composite powders at the nanoscale.

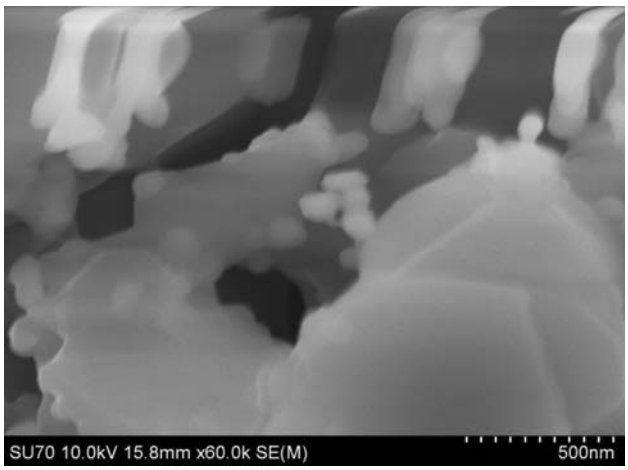

Fig. 13 Fracture Surface SEM image, ×60000, of HA containing 5 wt% ZrO_2 conventionally sintered at 1200°C

From Fig. 7 it is apparent that increased ZrO_2 loading decreases the relative density of the composites and that CS produces denser composites than MS. The densest materials are produced at 1200°C for both sintering regimes. The level of interconnected open porosity increased in the 0 wt% ZrO_2 MS samples compared to their CS counterparts, as shown in Figs. 8 and 11. It is also apparent that MS sintering and increased ZrO_2 content serves to increase the amount of open interconnected porosity (Figs. 8, 11). The CS samples with 5 wt% ZrO_2 additions exhibited 11% open porosity while their MS counterparts showed an increase of open porosity up to 16%. To summarise, the MS samples showed an increase in interconnected open porosity compared to the CS samples. Added to this, the interconnected open porosity increased with an increase in the ZrO_2 loadings while slightly affecting the mechanical properties at the same sintering temperature.

From the X ray diffraction data it is clear that TCP starts to form even with 0 wt% ZrO_2 as HA becomes unstable at approximately 1200°C [39]. The introduction of ZrO_2 into the composite results in an increase in the formation of TCP during sintering by up to four times the original amount obtained in the 0 wt% ZrO_2 samples sintered at 1200°C, with no general trend in HA degradation between the MS and CS samples. Evis [19] has shown that the reaction between HA and ZrO_2 results in HA decomposition and the formation of TCP at lower temperatures. The CaO released by the HA during sintering at 1200°C is used in the formation of calcium-stabilised cubic zirconia and/or calcium zirconate with accelerated degradation of HA.

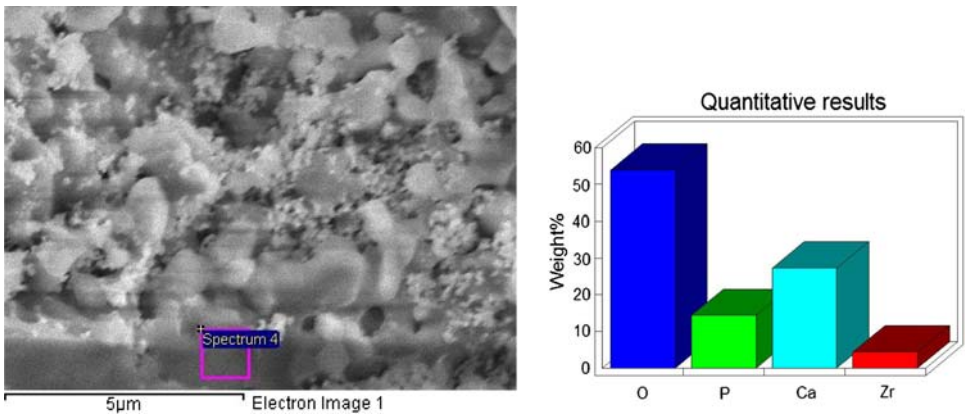

Fig. 14 SEM and EDX of a smooth, densified, area of HA + 5 wt% ZrO_2 conventionally sintered at 1200°C

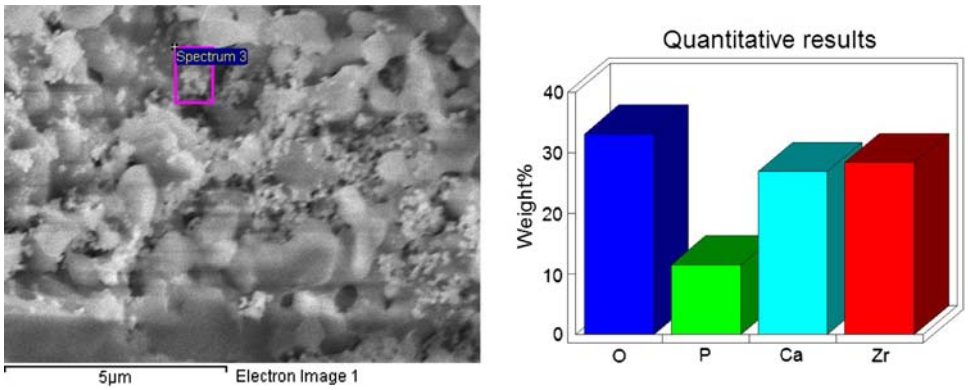

Fig. 15 SEM and EDX of a rough, porous, area of HA + 5 wt% ZrO_2 conventionally sintered at 1200°C

This can be seen in Table 2 where the amount of cubic ZrO_2 produced during sintering increases with increasing wt% ZrO_2 additions.

As with density, the hardness of the composites (Fig. 9) decreases with ZrO_2 content, and increases with sintering temperature. However, the MS composites are less hard than their CS counterparts; this is a reflection of the increased amount of open porosity present in the MS samples.

Due to the competing effects of increased densification and increased open porosity, there is little statistical difference in the strength of the composites as a result of heating method or ZrO_2 content. However, all composites show improvement in strength with increased sintering temperature.

The fracture surfaces and EDX data suggest that nano-sized ZrO_2 prevents the densification of the HA matrix by effectively pinning grain boundaries. This effect is more pronounced in the MS materials leading to an increase in the measured amount of open porosity.

The results of this study indicate that nano sized ZrO_2 is ineffective at strengthening a HA composite. It also indicates that the morphology of the material produced is dependent on the heating method employed. Microwave energy produces HA–ZrO_2 composites with similar strengths to those produced by conventional sintering but with a greater amount of open porosity. Increased interconnected open porosity is considered to be useful for biomedical applications as it can promote osteo-integration.

5 Conclusions

- Ball milling is sufficient to homogeneously disperse nanosize ZrO_2 in nano-HA.
- A sintering temperature of 700°C is insufficient to produce densified bodies.
- A sintering temperature of 1200°C produces the most dense bodies and hence stronger composites with levels of open porosity which are higher in microwave processed composites.
- Increased ZrO_2 loading effectively pins grain boundaries preventing complete densification.
- There is little difference in mechanical properties of the composites produced by either microwave or conventional heating at high sintering temperatures.
- Nano-sized ZrO_2 does not impart any extra strength to an HA matrix. Increased ZrO_2 loadings retard mechanical strength due to the increased formation of TCP and increasing porosity.
- The main difference between microwave and conventionalsintering is that materials with different microstructures are formed. The higher levels of interconnected

open porosity in MS HA–ZrO_2 composites are considered to be useful in promoting osteo-integration.

Acknowledgement This work was funded by Enterprise Ireland Technology Development Grant EI/TD/2006/0328.

References

1. Kalita SJ, Bhardwaj A, Bhatt HA. Nanocrystalline calcium phosphate ceramics in biomedical engineering. Mater Sci Eng C. 2006;27(3):441–9.
2. Prabakaran K, Kannan S, Rajeswari S. Development and characterisation of zirconia and hydroxyapatite composites for orthopaedic applications. Trends Biomater Artif Organs. 2005;18(2): 114–6.
3. Manley MT, Sutton K, Dumbleton J. Calcium phosphates: a survey of the orthopaedic literature. In: Epinette JA, Manley MT, editors. Fifteen years of clinical experience with hydroxyapatite coatings in joint arthroplasty. New York: Springer-Verlag; 2004. p. 452.
4. Itoh S, Kikuchi M, Takakuda K, Koyama Y, Matsumoto HN, Ichinose S, et al. The biocompatibility and osteoconductive activity of a novel hydroxyapatite/collagen composite biomaterial, and its function as a carrier of rhBMP-2. J Biomed Mater Res. 2000;54(3):445–53.
5. Anselme K, Noel B, Flautre B, Blary MC, Delecourt C, Descamps M, et al. Association of porous hydroxyapatite and bone marrow cells for bone regeneration. Bone. 1999;25(2):51S–4S.
6. Erbe EM, Marx JG, Clineff TD, Bellincampi LD. Potential of an ultraporous β-tricalcium phosphate synthetic cancellous bone void filler and bone marrow aspirate composite graft. Eur Spine J. 2001;10(2):S141–6.
7. Heimann RB, Vu TA. Effects of CaO on thermal decomposition during sintering of composite hydroxyapatite–zirconia mixtures for monolithic bioceramic implants. J Mater Sci Lett. 1997; 16(6):437–9.
8. White AA, Best SM, Kinloch IA. Hydroxyapatite-carbon nanotube composites for biomedical applications: a review. Int J Appl Ceram Technol. 2007;4(1):1–13.
9. Bernache-Assollant D, Ababou A, Champion E, Heughebaert M. Sintering of calcium phosphate hydroxyapatite $Ca_{10}(PO_4)_6(OH)_2$. I Calcination and grain growth. J Eur Ceram Soc. 2003;23(2):229–41.
10. Hing KA, Gibson IR, Di Silvio L, Best SM, Bonfield W. Effect of variation in Ca:P ratio on the cellular response of primary human osteoblast-like cells to hydroxyapatite-based ceramics. Bioceramics. 1998;11:293–6.
11. Nagarajan VS, Rao KJ. Structural, mechanical and biocompatibility studies of hydroxyapatite-derived composites toughened by zirconia addition. J Mater Chem. 1993;3(1):43–51.
12. Brosnan KH. Sintering of alumina parts with microwave energy. USA: The Pennsylvania State University; 2002. p. 67.
13. Ciacchi FT, Nightingale SA, Badwal SPS. Microwave sintering of zirconia–yttria electrolytes and measurements of their ionic conductivity. Solid State Ion. 1996;86–88(2):1167–72.
14. Masonis JL, Bourne RB, Ries MD, McCalden RW, Salehi A, Kelman DC. Zirconia femoral head fractures: a clinical and retrieval analysis. J Arthroplast. 2004;19(7):898–905.
15. DeAza AH, Chevalier J, Fantozzi G, Schehl M, Torrecillas R. Crack growth resistance of alumina, zirconia and zirconia toughened alumina ceramics for joint prostheses. Biomaterials. 2001; 23:937–45.
16. Kong Y, Yang Z, Zhang G, Yuan Q. Friction and wear characteristics of mullite. ZTM and TZP ceramics. Wear. 1998;218(2): 159–66.
17. Casellas D, Nagl MM, Llanes L, Anglada M. Fracture toughness of alumina and ZTA ceramics: microstructural coarsening effects. J Mater Process Technol. 2003;143–144:148–52.
18. Towler MR, Gibson IR. The effect of low levels of zirconia addition on the mechanical properties of hydroxyapatite. J Mater Sci Lett. 2001;20(18):1719–22.
19. Evis Z. Reactions in hydroxylapatite-zirconia composites. Ceram Int. 2006;33(6):987–91.
20. Ruys AJ, Wei M, Sorrell CC, Dickson MR, Brandwood A, Milthorpe BK. Sintering effects on the strength of hydroxyapatite. Biomaterials. 1995;16(5):409–15.
21. Upadhyaya DD, Ghosh A, Gurumurthy KR, Prasad R. Microwave sintering of cubic zirconia. Ceram Int. 2001;27(4):415–8.
22. Goldstein A, Travitzky N, Singurindy A, Kravchik M. Direct microwave sintering of yttria-stabilized zirconia at 245 GHz. J Eur Ceram Soc. 1999;19(12):2067–72.
23. Ramesh PD, Brandon D, Schachter L. Use of partially oxidized SiC particle bed for microwave sintering of low loss ceramics. Mater Sci Eng. 1999;266(1–2):211–20.
24. Vaidhyanathan B, Binner JGP. Densification of nanostructured YSZ green compacts. Key Eng Mater. 2004;246–248:2339–42.
25. Thostenson ET, Chou TW. Microwave processing: fundamentals and applications. Composites A. 1999;30(9):1055–71.
26. Clark DE, Folz DC, West JK. Processing materials with microwave energy. Mater Sci Eng A. 2000;287(2):153–8.
27. Karageorgiou V, Kaplan D. Porosity of 3D biomaterial scaffolds and osteogenesis. Biomaterials. 2005;26(7):5474–91.
28. Klenke FM, Liu Y, Yuan H, Hunziker EB, Siebenrock KA. Impact of pore size on the vascularization and osseointegration of ceramic bone substitutes in vivo. J Biomed Mater Res A. 2008;85(3):777–86.
29. Chang BS, Lee CK, Hong KS, Youn HJ, Ryu HS, Chung SS, et al. Osteoconduction at porous hydroxyapatite with various pore configurations. Biomaterials. 2000;21(12):1291–8.
30. Kuboki Y, Takita H, Kobayashi D, Tsuruga E, Inoue M, Murata M, et al. BMP-induced osteogenesis on the surface of hydroxyapatite with geometrically feasible and nonfeasible structures: topology of osteogenesis. J Biomed Mater Res A. 1998;39(2):190–9.
31. Jarcho M, Bolen CH, Thomas MB, Bobick J, Kay JF, Doremus RH. Hydroxylapatite synthesis and characterisation in dense polycrystalline form. J Mater Sci. 1976;11(11):2027–35.
32. Ingel RP, Lewis D III. Lattice parameters and density for Y_2O_3-stabilized ZrO_2. J Am Ceram Soc. 1986;69(4):325–32.
33. CEN. Dental ceramic (ISO 6872-1995). In: Standardization ECf, editor; 1998.
34. Evis Z, Usta M, Kutbay I. Hydroxyapatite and zirconia composites: effect of MgO and MgF_2 on the stability of phases and sinterability. Mater Chem Phys. 2008;110(1):68–75.
35. Gross KA, Berndt CC. Thermal processing of hydroxyapatite for coating production. J Biomed Mater Res. 1998;39(4):580–7.
36. Pontier C, Viana M, Champion E, Chulia D. Apatitic calcium phosphates used in compression: rationalisation of the end-use properties. Powder Technol. 2002;130:436–41.
37. Elliot JC. Structure and chemistry of the apatites and other calcium orthophosphates. Amsterdam: Elsevier; 1994.
38. Evis Z, Ergun C, Doremus RH. Hydroxylapatite–zirconia composites: thermal stability of phases and sinterability as related to the CaO–ZrO_2 phase diagram. J Mater Sci. 2005;40(5):1127–34.
39. Buys AJ, Sorrell CC, Brandwood A, Milthorpe BK. Hydroxyapatite sintering characteristics: correlation with powder morphology bv high-resolution microscopy. J Mater Sci Lett. 1995; 14(10):744–7.